The importance of coarse levels for domain decomposition methods

Alexander Heinlein[1]

International Conference on Preconditioning Techniques for Scientific and Industrial Applications (Preconditioning 2024), Georgia Institute of Technology, Atlanta, USA, June 10–12, 2024

[1]Delft University of Technology

Outline

1. One- and Two-Level Schwarz Preconditioners
2. The FROSCH Package – Algebraic and Parallel Schwarz Preconditioners in TRILINOS
3. Coarse Spaces for Some Challenging Problems
4. Multilevel Domain Decomposition for Neural Networks

One- and Two-Level Schwarz Preconditioners

Solving A Model Problem

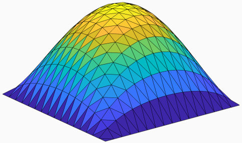

$\alpha(x) = 1$

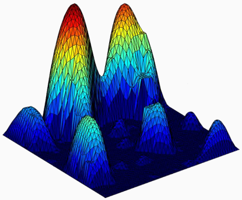

heterogeneous $\alpha(x)$

Consider a **diffusion model problem**:

$$-\nabla \cdot (\alpha(x) \nabla u(x)) = f \quad \text{in } \Omega = [0,1]^2,$$
$$u = 0 \quad \text{on } \partial\Omega.$$

Discretization using finite elements yields a **sparse** linear system of equations

$$\boldsymbol{K}\boldsymbol{u} = \boldsymbol{f}.$$

Direct solvers

For fine meshes, solving the system using a direct solver is not feasible due to **superlinear complexity and memory cost**.

Iterative solvers

Iterative solvers are efficient for solving sparse linear systems of equations, however, the **convergence rate generally depends on the condition number** $\kappa(\boldsymbol{K})$. It deteriorates, e.g., for

- fine meshes, that is, small element sizes h
- large contrasts $\frac{\max_x \alpha(x)}{\min_x \alpha(x)}$

$\Rightarrow$ We introduce a preconditioner $\boldsymbol{M}^{-1} \approx \boldsymbol{K}^{-1}$ to improve the condition number:

$$\boldsymbol{M}^{-1}\boldsymbol{K}\boldsymbol{u} = \boldsymbol{M}^{-1}\boldsymbol{f}$$

Two-Level Schwarz Preconditioners

One-level Schwarz preconditioner

Overlap $\delta = 1h$

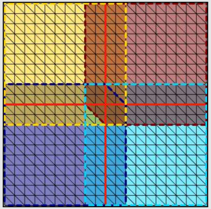

Solution of local problem

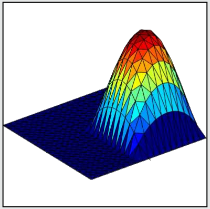

Based on an **overlapping domain decomposition**, we define a **one-level Schwarz operator**

$$M_{\text{OS-1}}^{-1} K = \sum_{i=1}^{N} R_i^\top K_i^{-1} R_i K,$$

where R_i and $R_i^\top$ are restriction and prolongation operators corresponding to Ω_i', and $K_i := R_i K R_i^\top$.

Condition number estimate:

$$\kappa \left(M_{\text{OS-1}}^{-1} K \right) \leq C \left(1 + \frac{1}{H\delta} \right)$$

with subdomain size H and overlap width δ.

Lagrangian coarse space

Coarse triangulation

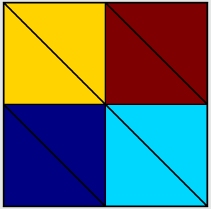

Coarse solution

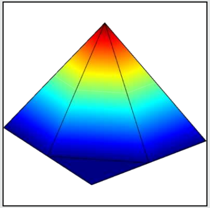

The **two-level overlapping Schwarz operator** reads

$$M_{\text{OS-2}}^{-1} K = \underbrace{\Phi K_0^{-1} \Phi^\top K}_{\text{coarse level – global}} + \underbrace{\sum_{i=1}^{N} R_i^\top K_i^{-1} R_i K}_{\text{first level – local}},$$

where Φ contains the coarse basis functions and $K_0 := \Phi^\top K \Phi$; cf., e.g., **Toselli, Widlund (2005)**. The construction of a Lagrangian coarse basis requires a coarse triangulation.

Condition number estimate:

$$\kappa \left(M_{\text{OS-2}}^{-1} K \right) \leq C \left(1 + \frac{H}{\delta} \right)$$

One-level Schwarz preconditioner

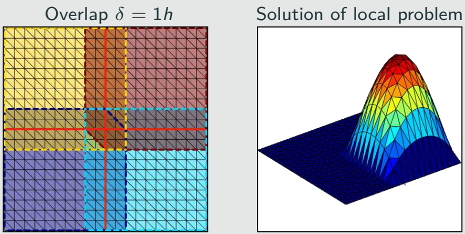

Lagrangian coarse space

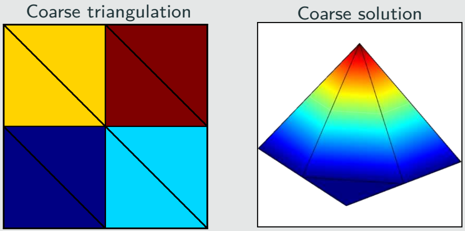

Diffusion model problem in two dimensions,
$H/h = 100$

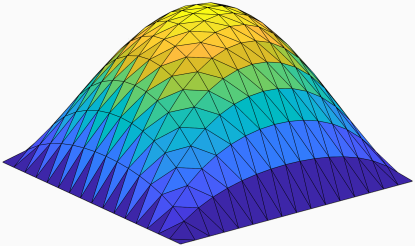

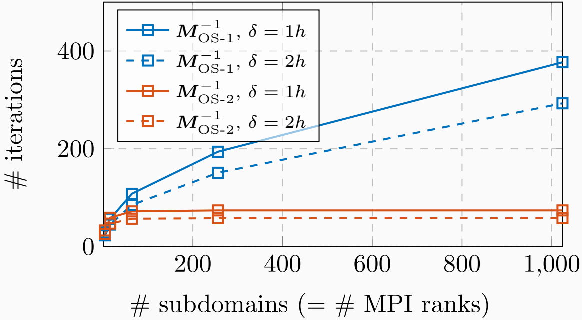

The FROSch Package – Algebraic and Parallel Schwarz Preconditioners in Trilinos

FROSch (Fast and Robust Overlapping Schwarz) Framework in Trilinos

Software

- Object-oriented C++ domain decomposition solver framework with MPI-based distributed memory parallelization
- Part of TRILINOS with support for both parallel linear algebra packages EPETRA and TPETRA
- Node-level parallelization and performance portability on CPU and GPU architectures through KOKKOS and KOKKOSKERNELS
- Accessible through unified TRILINOS solver interface STRATIMIKOS

Methodology

- **Parallel scalable multi-level Schwarz domain decomposition preconditioners**
- **Algebraic construction** based on the parallel distributed system matrix
- **Extension-based coarse spaces**

Team (active)

- Filipe Cumaru (TU Delft)
- Kyrill Ho (UCologne)
- Jascha Knepper (UCologne)
- Friederike Röver (TUBAF)
- Lea Saßmannshausen (UCologne)
- Alexander Heinlein (TU Delft)
- Axel Klawonn (UCologne)
- Siva Rajamanickam (SNL)
- Oliver Rheinbach (TUBAF)
- Ichitaro Yamazaki (SNL)

The **energy-minimizing extension** $v_i = H_{\partial\Omega_i \to \Omega_i}(v_{i,\partial\Omega_i})$ solves

$$\begin{aligned} -\Delta v_i &= 0 && \text{in } \Omega_i, \\ v_i &= v_{i,\partial\Omega_i} && \text{on } \partial\Omega_i. \end{aligned}$$

Hence, $v_i = E_{\partial\Omega_i \to \Omega_i}(\mathbb{1}_{\partial\Omega_i}) = \mathbb{1}$.

Due to **linearity of the extension operator**, we have

$$\sum_i \varphi_i = \mathbb{1}_{\partial\Omega_i} \Rightarrow \sum_i E_{\partial\Omega_i \to \Omega_i}(\varphi_i) = \mathbb{1}_{\Omega_i}$$

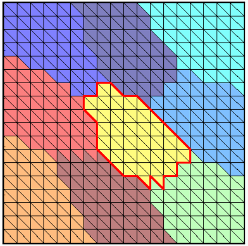

Null space property

Any extension-based coarse space built from a partition of unity on the domain decomposition interface satisfies the **null space property necessary for numerical scalability**:

$\sum_{\text{edges} \subset \partial\Omega_i}$ 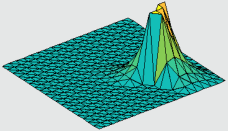 $+ \sum_{\text{vertices} \subset \partial\Omega_i}$ 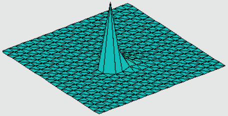 $=$ 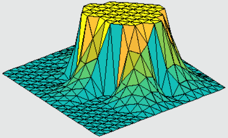

Algebraicity of the energy-minimizing extension

The computation of energy-minimizing extensions only requires $\boldsymbol{K}_{II}$ and $\boldsymbol{K}_{I\Gamma}$, **submatrices of the fully assembled matrix** $\boldsymbol{K}_i$.

$$\boldsymbol{v} = \begin{bmatrix} -\boldsymbol{K}_{II}^{-1}\boldsymbol{K}_{I\Gamma} \\ \boldsymbol{I}_\Gamma \end{bmatrix} \boldsymbol{v}_\Gamma,$$

Algorithmic Framework for FROSch Preconditioners

Overlapping domain decomposition

The **overlapping subdomains** are constructed by **recursively adding layers of elements** via the sparsity pattern of $\boldsymbol{K}$.

The corresponding matrices

$$\boldsymbol{K}_i = \boldsymbol{R}_i \boldsymbol{K} \boldsymbol{R}_i^T$$

can easily be extracted from $\boldsymbol{K}$.

Nonoverlapping DD

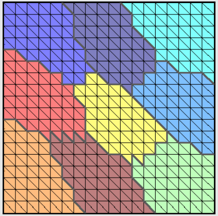

Algorithmic Framework for FROSch Preconditioners

Overlapping domain decomposition

The **overlapping subdomains** are constructed by **recursively adding layers of elements** via the sparsity pattern of $\boldsymbol{K}$.

The corresponding matrices

$$\boldsymbol{K}_i = \boldsymbol{R}_i \boldsymbol{K} \boldsymbol{R}_i^T$$

can easily be extracted from $\boldsymbol{K}$.

Nonoverlapping DD

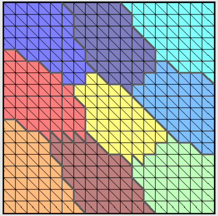

Overlap $\delta = 1h$

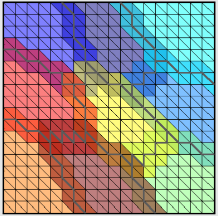

Overlapping domain decomposition

The **overlapping subdomains** are constructed by **recursively adding layers of elements** via the sparsity pattern of $\boldsymbol{K}$.

The corresponding matrices

$$\boldsymbol{K}_i = \boldsymbol{R}_i \boldsymbol{K} \boldsymbol{R}_i^T$$

can easily be extracted from $\boldsymbol{K}$.

Nonoverlapping DD

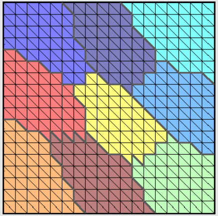

Overlap $\delta = 1h$

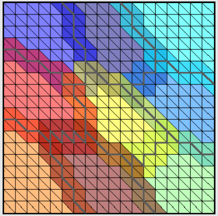

Overlap $\delta = 2h$

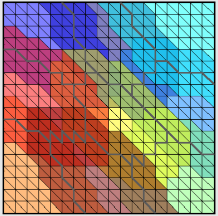

Overlapping domain decomposition

The **overlapping subdomains** are constructed by **recursively adding layers of elements** via the sparsity pattern of $\boldsymbol{K}$.

The corresponding matrices

$$\boldsymbol{K}_i = \boldsymbol{R}_i \boldsymbol{K} \boldsymbol{R}_i^T$$

can easily be extracted from $\boldsymbol{K}$.

Nonoverlapping DD

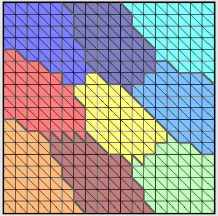

Overlap $\delta = 1h$

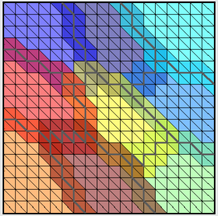

Overlap $\delta = 2h$

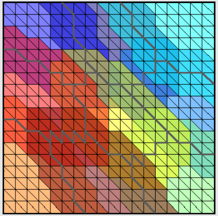

Coarse space

1. Interface components

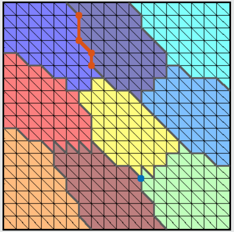

Algorithmic Framework for FROSch Preconditioners

Overlapping domain decomposition

The **overlapping subdomains** are constructed by **recursively adding layers of elements** via the sparsity pattern of $\boldsymbol{K}$.

The corresponding matrices

$$\boldsymbol{K}_i = \boldsymbol{R}_i \boldsymbol{K} \boldsymbol{R}_i^T$$

can easily be extracted from $\boldsymbol{K}$.

Nonoverlapping DD

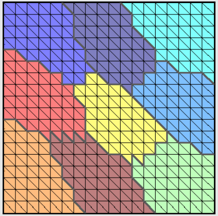

Overlap $\delta = 1h$

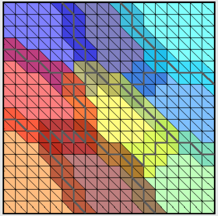

Overlap $\delta = 2h$

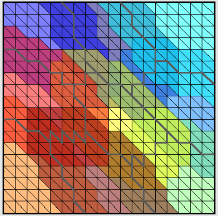

Coarse space

1. Interface components

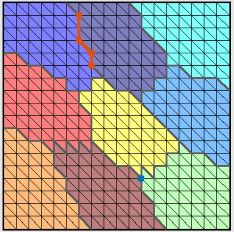

2. Interface basis (partition of unity $\times$ null space)

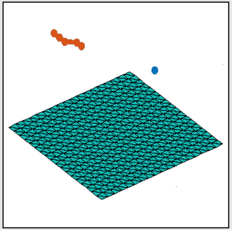

For **scalar elliptic problems**, the **null space** consists only of **constant functions**.

Algorithmic Framework for FROSch Preconditioners

Overlapping domain decomposition

The **overlapping subdomains** are constructed by **recursively adding layers of elements** via the sparsity pattern of $\boldsymbol{K}$.

The corresponding matrices

$$\boldsymbol{K}_i = \boldsymbol{R}_i \boldsymbol{K} \boldsymbol{R}_i^T$$

can easily be extracted from $\boldsymbol{K}$.

Nonoverlapping DD

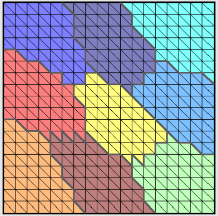

Overlap $\delta = 1h$

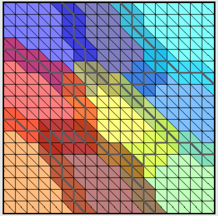

Overlap $\delta = 2h$

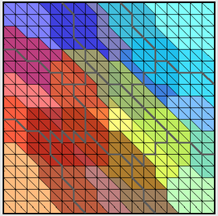

Coarse space

1. Interface components

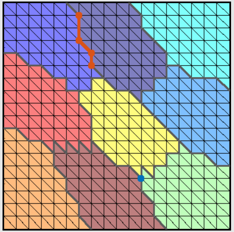

2. Interface basis (partition of unity $\times$ null space)

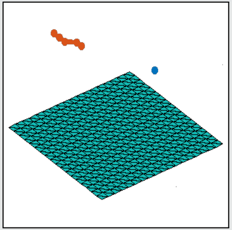

For **scalar elliptic problems**, the **null space** consists only of **constant functions**.

3. Extension

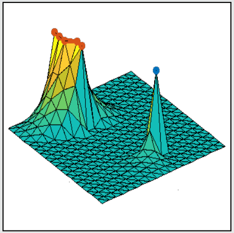

Examples of FROSch Coarse Spaces

GDSW (Generalized Dryja–Smith–Widlund)

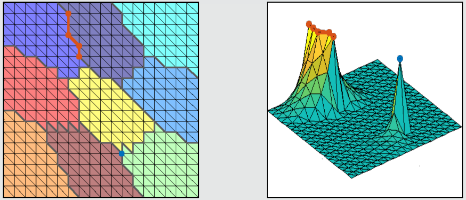

- Dohrmann, Klawonn, Widlund (2008)
- Dohrmann, Widlund (2009, 2010, 2012)

RGDSW (Reduced dimension GDSW)

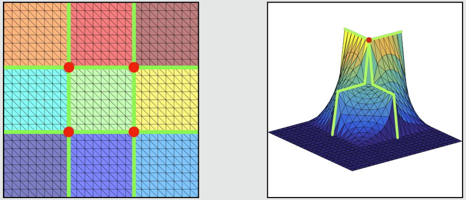

- Dohrmann, Widlund (2017)
- H., Klawonn, Knepper, Rheinbach, Widlund (2022)

MsFEM (Multiscale Finite Element Method)

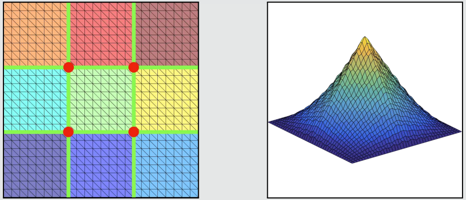

- Hou (1997), Efendiev and Hou (2009)
- Buck, Iliev, and Andrä (2013)
- H., Klawonn, Knepper, Rheinbach (2018)

Q1 Lagrangian / piecewise bilinear

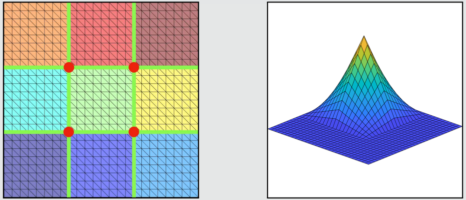

Piecewise linear interface partition of unity functions and a **structured domain decomposition**.

Weak Scalability up to $64\,\mathrm{k}$ MPI Ranks / $1.7\,\mathrm{b}$ Unknowns (3D Poisson; Juqueen)

GDSW vs RGDSW (reduced dimension)

Heinlein, Klawonn, Rheinbach, Widlund (2019).

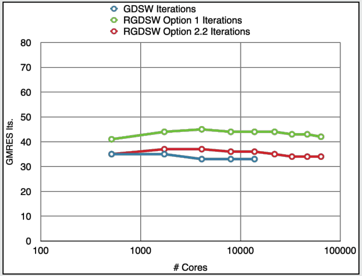

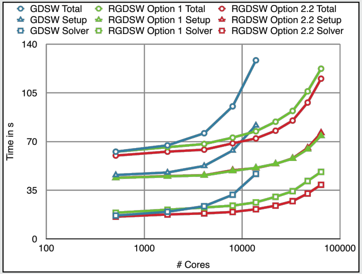

Two-level vs three-level GDSW

Heinlein, Klawonn, Rheinbach, Röver (2019, 2020).

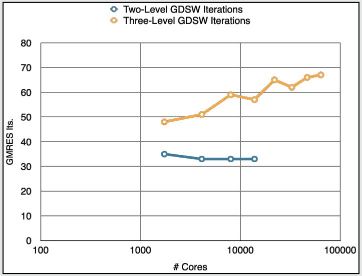

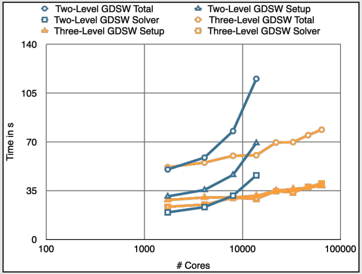

Coarse Spaces for Some Challenging Problems

Spectral Extension-Based Coarse Spaces for Schwarz Preconditioners

Highly heterogeneous problems ...

...appear in most areas of modern science and engineering:

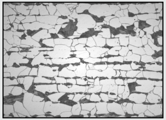

Micro section of a dual-phase steel. Courtesy of **J. Schröder**.

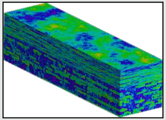

Groundwater flow (SPE10); cf. **Christie and Blunt (2001)**.

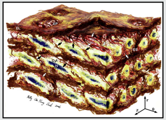

Composition of arterial walls; taken from **O'Connell et al. (2008)**.

Spectral coarse spaces

The coarse space is **enhanced** by eigenfunctions of **local edge and face eigenvalue problems** with eigenvalues below tolerances $tol_{\mathcal{E}}$ and $tol_{\mathcal{F}}$:

$$\kappa\left(M_*^{-1}K\right) \leq C\left(1 + \frac{1}{tol_{\mathcal{E}}} + \frac{1}{tol_{\mathcal{F}}} + \frac{1}{tol_{\mathcal{E}} \cdot tol_{\mathcal{F}}}\right);$$

C does not depend on h, H, or the coefficients.
OS-ACMS & **adaptive GDSW (AGDSW)** (**Heinlein, Klawonn, Knepper, Rheinbach (2018, 2018, 2019)**).

Related works (non-exhaustive)

- **FETI & Neumann–Neumann:** **Bjørstad and Krzyzanowski (2002); Bjørstad, Koster, and Krzyzanowski (2001); Rixen and Spillane (2013); Spillane (2015, 2016)** ...
- **BDDC & FETI-DP:** **Mandel and Sousedík (2007); Sousedík (2010); Sístek, Mandel, and Sousedík (2012); Dohrmann and Pechstein (2013, 2016); Klawonn, Radtke, and Rheinbach (2014, 2015, 2016); Klawonn, Kühn, and Rheinbach (2015, 2016, 2017); Kim and Chung (2015); Kim, Chung, and Wang (2017); Beirão da Veiga et al. (2017); Calvo and Widlund (2016); Oh et al. (2017)** ...
- **Overlapping Schwarz:** **Galvis and Efendiev (2010, 2011); Nataf, Xiang, Dolean, and Spillane (2011); Spillane, Dolean, Hauret, Nataf, Pechstein, and Scheichl (2011); Gander, Loneland, and Rahman (preprint 2015); Eikeland, Marcinkowski, and Rahman (TR 2016); Marcinkowski and Rahman (2018)** ...
- **Spectral AMGe (ρAMGe):** **Chartier, Falgout, Henson, Jones, Manteuffel, McCormick, Ruge, and Vassilevski (2003)**
...

Local eigenvalue problems

Local generalized eigenvalue problems corresponding to the edges $\mathcal{E}$ and faces $\mathcal{F}$ of the domain decomposition:

$$\forall E \in \mathcal{E}: \qquad \boldsymbol{S}_{EE}\tau_{*,E} = \lambda_{*,E}\boldsymbol{K}_{EE}\tau_{*,E}, \quad \forall \tau_{*,E} \in V_E,$$
$$\forall F \in \mathcal{F}: \qquad \boldsymbol{S}_{FF}\tau_{*,F} = \lambda_{*,F}\boldsymbol{K}_{FF}\tau_{*,F}, \quad \forall \tau_{*,F} \in V_F,$$

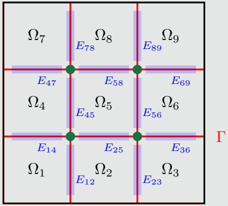

with **Schur complements** S_{EE}, S_{FF} with **Neumann boundary conditions** and **submatrices** K_{EE}, K_{FF} of K. We select eigenfunctions corresponding to **eigenvalues below tolerances** $tol_{\mathcal{E}}$ and $tol_{\mathcal{F}}$.

→ The corresponding coarse basis functions are **energy-minimizing extensions** into the interior of the subdomains.

Extensions in the generalized eigenvalue problem

Blue $\alpha = 1$; yellow $\alpha = 10^6$

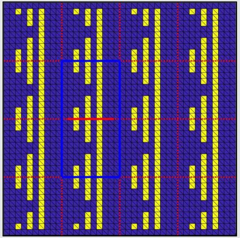

Low energy extension $\boldsymbol{S}_{EE}$

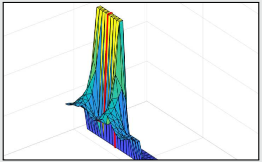

High energy extension $\boldsymbol{K}_{EE}$

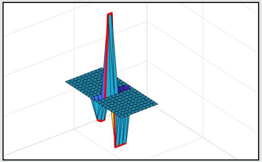

Coarse basis function

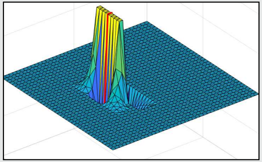

The extensions on the two sides of the generalized eigenvalue problem correspond to **low and high energy extensions of the trace** → detects coefficient jumps.

Highly heterogeneous problems ...

...appear in most areas of modern science and engineering:

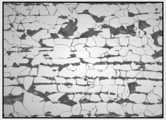

Micro section of a dual-phase steel. Courtesy of **J. Schröder**.

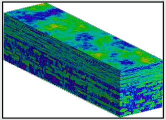

Groundwater flow (SPE10); cf. **Christie and Blunt (2001)**.

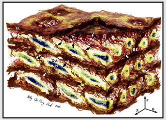

Composition of arterial walls; taken from **O'Connell et al. (2008)**.

Spectral coarse spaces

The coarse space is **enhanced** by eigenfunctions of **local edge and face eigenvalue problems** with eigenvalues below tolerances $tol_{\mathcal{E}}$ and $tol_{\mathcal{F}}$:

$$\kappa\left(M_*^{-1}K\right) \leq C\left(1 + \frac{1}{tol_{\mathcal{E}}} + \frac{1}{tol_{\mathcal{F}}} + \frac{1}{tol_{\mathcal{E}} \cdot tol_{\mathcal{F}}}\right);$$

C does not depend on h, H, or the coefficients.

OS-ACMS & **adaptive GDSW (AGDSW)** (**Heinlein, Klawonn, Knepper, Rheinbach (2018, 2018, 2019)**).

Foam coefficient function example

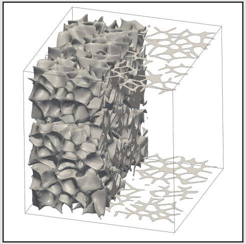

Solid phase: $\alpha = 10^6$; **transparent phase:** $\alpha = 1$; 100 subdomains

V_0	$tol_{\mathcal{E}}$	$tol_{\mathcal{F}}$	it.	κ	dim V_0	dim V_0/ dof
V_{GDSW}	—	—	**565**	$1.3\cdot 10^6$	1 601	0.27 %
V_{AGDSW}	0.05	0.05	**60**	30.2	1 968	0.33 %
$V_{\mathrm{OS-ACMS}}$	0.001	0.001	**57**	30.3	690	0.12 %

Cf. **Heinlein, Klawonn, Knepper, Rheinbach (2018, 2019)**.

Two algebraic eigenvalue problems

Use the a-orthogonal decomposition

$$V_{\Omega_e} = V^0_{\Omega_e} \oplus \{E_{\partial\Omega_e \to \Omega_e}(v) : v \in V_{\partial\Omega_e}\}$$

to ***"split the AGDSW (Neumann) eigenvalue problem"*** into two:

- **Dirichlet eigenvalue problem** on $V^0_{\Omega_e}$
- **Transfer eigenvalue problem** on $V_{\Omega_e,\text{harm}}$; cf. **Smetana, Patera (2016)**

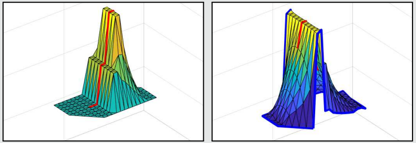

Condition number estimate

$$\kappa\left(\boldsymbol{M}^{-1}_{\text{DIR\&TR}}\boldsymbol{K}\right) \leq C \max\left\{{}^{1}/_{TOL_{\text{DIR}}}, {}^{TOL_{\text{TR}}}/_{\alpha_{\min}}\right\},$$

where C is independent of H, h, and the contrast of the coefficient function α.

Heinlein & Smetana (subm. 2023; preprint arXiv).

Numerical results – SPE10 benchmark

Layer 70 from model 2; cf. **Christie and Blunt (2001)**

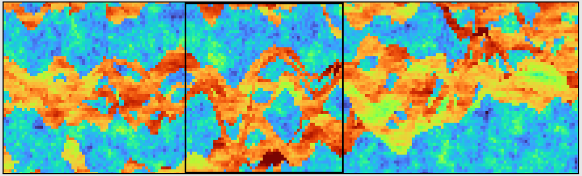

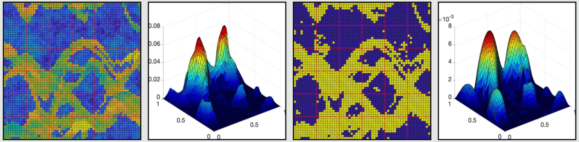

V_0	TOL_{DIR}	TOL_{TR}	dim V_0	κ	its.
V_{GDSW}	-	-	85	$2.0\cdot10^{5}$	57
V_{AGDSW}	$1.0\cdot10^{-2}$		93	19.3	38
$V_{\text{DIR\&TR}-a}$	$1.0\cdot10^{-3}$	$1.0\cdot10^{5}$	90	19.4	39
$V_{\text{DIR\&TR}-l^2}$	$1.0\cdot10^{-3}$	$1.0\cdot10^{5}$	147	9.6	31
Original coefficient (without thresholding)					
V_{GDSW}	-	-	85	20.6	42

Linear & Nonlinear Preconditioning

Let us consider the nonlinear problem arising from the discretization of a partial differential equation

$$\boldsymbol{F}\left(\boldsymbol{u}\right) = 0.$$

We solve the problem using a **Newton-Krylov approach**, i.e., we solve a sequence of linearized problems using a Krylov subspace method:

$$D\boldsymbol{F}\left(\boldsymbol{u}^{(k)}\right) \Delta \boldsymbol{u}^{(k+1)} = \boldsymbol{F}\left(\boldsymbol{u}^{(k)}\right).$$

Linear preconditioning

In linear preconditioning, we **improve the convergence speed of the linear solver** by constructing a **linear operator** $\boldsymbol{M}^{-1}$ and solve linear systems

$$\boldsymbol{M}^{-1} D\boldsymbol{F}\left(\boldsymbol{u}^{(k)}\right) \Delta \boldsymbol{u}^{(k+1)} = \boldsymbol{M}^{-1} \boldsymbol{F}(\boldsymbol{u}^{(k)}).$$

Goal:

- $\kappa\left(\boldsymbol{M}^{-1} D\boldsymbol{F}\left(\boldsymbol{u}^{(k)}\right)\right) \approx 1.$

$\Rightarrow \boldsymbol{M}^{-1} D\boldsymbol{F}\left(\boldsymbol{u}^{(k)}\right) \approx \boldsymbol{I}.$

Nonlinear preconditioning

In nonlinear preconditioning, we **improve the convergence speed of the nonlinear solver** by constructing a **nonlinear operator** G and solve the nonlinear system

$$\left(\boldsymbol{G} \circ \boldsymbol{F}\right)\left(\boldsymbol{u}\right) = 0.$$

Goals:

- $\boldsymbol{G} \circ \boldsymbol{F}$ almost linear.
- Additionally: $\kappa\left(D\left(\boldsymbol{G} \circ \boldsymbol{F}\right)\left(\boldsymbol{u}\right)\right) \approx 1.$

Linear & Nonlinear Preconditioning

Let us consider the nonlinear problem arising from the discretization of a partial differential equation

$$\boldsymbol{F}(\boldsymbol{u}) = 0.$$

We solve the problem using a **Newton-Krylov approach**, i.e., we solve a sequence of linearized problems using a Krylov subspace method:

$$D\boldsymbol{F}\left(\boldsymbol{u}^{(k)}\right)\Delta\boldsymbol{u}^{(k+1)} = \boldsymbol{F}\left(\boldsymbol{u}^{(k)}\right).$$

Linear preconditioning

In linear preconditioning, we **improve the convergence speed of the linear solver** by constructing a **linear operator** $\boldsymbol{M}^{-1}$ and solve linear systems

$$\boldsymbol{M}^{-1}D\boldsymbol{F}\left(\boldsymbol{u}^{(k)}\right)\Delta\boldsymbol{u}^{(k+1)} = \boldsymbol{M}^{-1}\boldsymbol{F}(\boldsymbol{u}^{(k)}).$$

Goal:

- $\kappa\left(\boldsymbol{M}^{-1}D\boldsymbol{F}\left(\boldsymbol{u}^{(k)}\right)\right) \approx 1.$

$\Rightarrow \boldsymbol{M}^{-1}D\boldsymbol{F}\left(\boldsymbol{u}^{(k)}\right) \approx \boldsymbol{I}.$

Nonlinear preconditioning

In nonlinear preconditioning, we **improve the convergence speed of the nonlinear solver** by constructing a **nonlinear operator** G and solve the nonlinear system

$$(\boldsymbol{G} \circ \boldsymbol{F})(\boldsymbol{u}) = 0.$$

Goals:

- $\boldsymbol{G} \circ \boldsymbol{F}$ almost linear.
- Additionally: $\kappa\left(D\left(\boldsymbol{G} \circ \boldsymbol{F}\right)(\boldsymbol{u})\right) \approx 1.$

Nonlinear Schwarz Methods

Two-level ASPEN & ASPIN methods

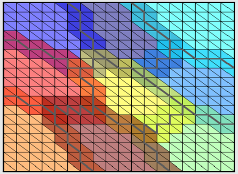

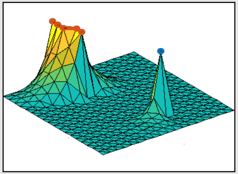

In **additive Schwarz preconditioned (in)exact Newton (ASPEN/ASPIN)** **(Cai and Keyes (2002))**, the nonlinear problem is modified

$$\boldsymbol{F}(\boldsymbol{u}) = 0 \Leftrightarrow \sum_{i=0}^{N} \boldsymbol{R}_i^T \boldsymbol{T}_i(\boldsymbol{u}) = 0$$

with corrections $\boldsymbol{T}_i(\boldsymbol{u})$ given by **nonlinear problems** on the **overlapping subdomains** / **coarse space**

$$\boldsymbol{R}_i \boldsymbol{F}(\boldsymbol{u} - \boldsymbol{R}_i^T \boldsymbol{T}_i(\boldsymbol{u})) = 0.$$

Coarse space via **Galerkin projection**: **Heinlein, Lanser (2020)**

More: **MS6 & MS11** *Nonlinear Preconditioning Techniques and Applications I & II*

Problem configuration

p-**Laplacian model problem** $(p = 4)$

$$\begin{aligned} -\alpha \Delta_p u &= 1 \quad \text{in } \Omega, \\ u &= 0 \quad \text{on } \partial\Omega. \end{aligned}$$

with $\alpha \Delta_p u := \text{div}(\alpha |\nabla u|^{p-2} \nabla u)$ on a **domain decomposition into** 6×6 **subdomains** with $H/h = 32$ and overlap $1h$.

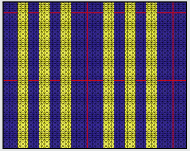

yellow: $\alpha = 10^3$
blue: $\alpha = 1$

no globalization						
size cp	**method**	**coarse space**	**outer it.**	**local it. (avg.)**	**coarse it.**	**GMRES it. (sum)**
145	ASPEN	AGDSW	5	27.0	35	77
25	ASPEN	MsFEM	>20	-	-	-
145	NK-AS	AGDSW	>20	-	-	-
Inexact Newton backtracking (INB) **Eisenstat and Walker (1994)**						
145	ASPEN	AGDSW	5	24.8	21	77
25	ASPEN	MsFEM	**18**	**83.9**	**75**	**852**
145	NK-AS	AGDSW	**13**	-	-	207

Cf. **Heinlein, Klawonn, Lanser (2022)**

Consider the discrete saddle point problem

$$\mathcal{A}x = \begin{bmatrix} \boldsymbol{K} & \boldsymbol{B}^\top \\ \boldsymbol{B} & \boldsymbol{0} \end{bmatrix} \begin{bmatrix} \boldsymbol{u} \\ \boldsymbol{p} \end{bmatrix} = \begin{bmatrix} \boldsymbol{f} \\ \boldsymbol{0} \end{bmatrix} = \mathcal{b}.$$

Monolithic GDSW preconditioner

We construct a **monolithic GDSW preconditioner**

$$\mathcal{M}_{\text{GDSW}}^{-1} = \phi \mathcal{A}_0^{-1} \phi^\top + \sum\nolimits_{i=1}^{N} \mathcal{R}_i^\top \overline{\mathcal{P}}_i \mathcal{A}_i^{-1} \mathcal{R}_i,$$

with block matrices $\mathcal{A}_0 = \phi^\top \mathcal{A} \phi$, $\mathcal{A}_i = \mathcal{R}_i \mathcal{A} \mathcal{R}_i^\top$, local pressure projections $\overline{\mathcal{P}}_i$, and

$$\mathcal{R}_i = \begin{bmatrix} \mathcal{R}_{u,i} & \boldsymbol{0} \\ \boldsymbol{0} & \mathcal{R}_{p,i} \end{bmatrix} \quad \text{and} \quad \phi = \begin{bmatrix} \Phi_{u,u_0} & \Phi_{u,p_0} \\ \Phi_{p,u_0} & \Phi_{p,p_0} \end{bmatrix}.$$

Using $\mathcal{A}$ to compute extensions: $\phi_I = -\mathcal{A}_{II}^{-1} \mathcal{A}_{I\Gamma} \phi_\Gamma$; cf. **Heinlein, Hochmuth, Klawonn (2019, 2020)**.

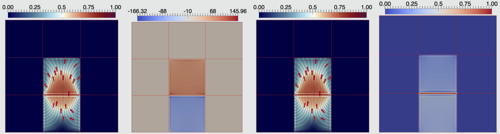

Φ_{u,u_0} Φ_{p,u_0} Φ_{u,p_0} Φ_{p,p_0}

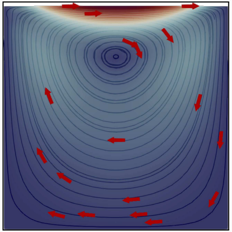

Stokes flow

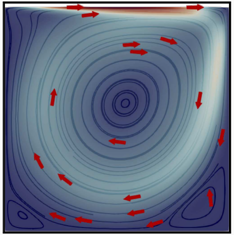

Navier–Stokes flow

Related work:

- Original work on monolithic Schwarz preconditioners: **Klawonn and Pavarino (1998, 2000)**
- Other publications on monolithic Schwarz preconditioners: e.g., **Hwang and Cai (2006)**, **Barker and Cai (2010)**, **Wu and Cai (2014)**, and the presentation **Dohrmann (2010)** at the *Workshop on Adaptive Finite Elements and Domain Decomposition Methods* in Milan.

Monolithic (R)GDSW Preconditioners for CFD Simulations

Consider the discrete saddle point problem

$$\mathcal{A}x = \begin{bmatrix} \boldsymbol{K} & \boldsymbol{B}^\top \\ \boldsymbol{B} & \boldsymbol{0} \end{bmatrix} \begin{bmatrix} \boldsymbol{u} \\ \boldsymbol{p} \end{bmatrix} = \begin{bmatrix} \boldsymbol{f} \\ \boldsymbol{0} \end{bmatrix} = \mathcal{b}.$$

Monolithic GDSW preconditioner

We construct a **monolithic GDSW preconditioner**

$$\mathcal{M}_{\text{GDSW}}^{-1} = \phi \mathcal{A}_0^{-1} \phi^\top + \sum_{i=1}^{N} \mathcal{R}_i^\top \overline{\mathcal{P}}_i \mathcal{A}_i^{-1} \mathcal{R}_i,$$

with block matrices $\mathcal{A}_0 = \phi^\top \mathcal{A} \phi$, $\mathcal{A}_i = \mathcal{R}_i \mathcal{A} \mathcal{R}_i^\top$.

SIMPLE block preconditioner

We employ the **SIMPLE (Semi-Implicit Method for Pressure Linked Equations)** block preconditioner

$$\mathcal{M}_{\text{SIMPLE}}^{-1} = \begin{bmatrix} \boldsymbol{I} & -\boldsymbol{D}^{-1}\boldsymbol{B} \\ 0 & \alpha \boldsymbol{I} \end{bmatrix} \begin{bmatrix} \boldsymbol{K}^{-1} & 0 \\ -\hat{\boldsymbol{S}}^{-1}\boldsymbol{B}\boldsymbol{K}^{-1} & \hat{\boldsymbol{S}}^{-1} \end{bmatrix};$$

see **Patankar and Spalding (1972)**. Here,

- $\hat{\boldsymbol{S}} = -\boldsymbol{B}\boldsymbol{D}^{-1}\boldsymbol{B}^\top$, with $\boldsymbol{D} = \operatorname{diag} \boldsymbol{K}$
- α is an under-relaxation parameter

We **approximate the inverses** using (R)GDSW preconditioners.

Monolithic vs. SIMPLE preconditioner

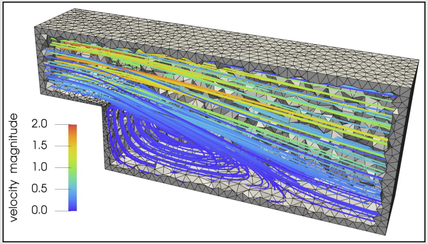

Steady-state Navier–Stokes equations

prec.	# MPI ranks	243	1 125	15 562
Monolithic RGDSW (FROSch)	setup	39.6 s	57.9 s	95.5 s
	solve	57.6 s	69.2 s	74.9 s
	total	**97.2 s**	**127.7 s**	**170.4 s**
SIMPLE RGDSW (Teko & FROSch)	setup	39.2 s	38.2 s	68.6 s
	solve	86.2 s	106.6 s	127.4 s
	total	125.4 s	144.8 s	196.0 s

Computations on Piz Daint (CSCS). Implementation in the finite element software `FEDDLib`.

Balancing the Velocity and Pressure Coarse Spaces

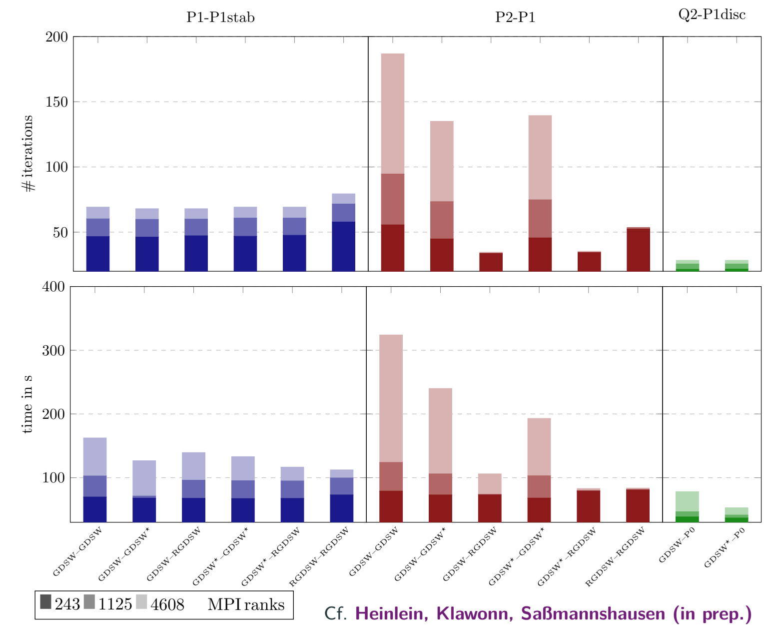

Cf. **Heinlein, Klawonn, Saßmannshausen (in prep.)**

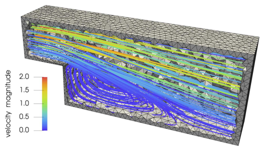

Varying the POU

GDSW:

GDSW*:

RGDSW:

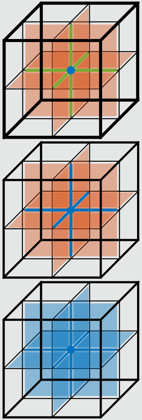

Results for Blood Flow Simulations

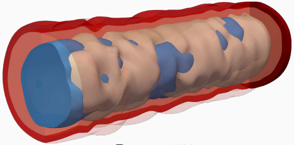

- **3D unsteady flow simulation** within the **geometry of a realistic artery** (from **Balzani et al. (2012)**) and kinematic viscosity $\nu = 0.03\,\mathrm{cm}^2/\mathrm{s}$
- **Parabolic inflow profile** is prescribed at inlet of geometry
- **Time discretization**: BDF-2; **space discretization**: P2-P1 elements

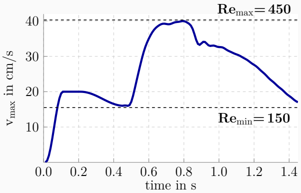

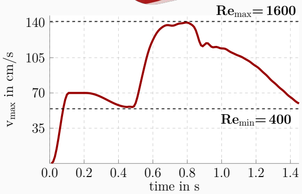

prec.	# MPI ranks	16	64	256
Monolithic RGDSW (FROSch)	avg. #its.	33	31	30
	setup	4 825 s	1 422 s	701 s
	solve	3 198 s	1 004 s	463 s
	total	8 023 s	2 426 s	**1 164 s**
SIMPLE RGDSW (Teko & FROSch)	avg. #its.	82	82	87
	setup	3 046 s	824 s	428 s
	solve	4 679 s	1 533 s	801 s
	total	**7 725 s**	**2 357 s**	1 229 s

prec.	# MPI ranks	16	64	256
Monolithic RGDSW (FROSch)	avg. #its.	36	36	36
	setup	4 808 s	1 448 s	688 s
	solve	3 490 s	1 186 s	538 s
	total	**8 298 s**	**2 634 s**	**1 226 s**
SIMPLE RGDSW (Teko & FROSch)	avg. #its.	157	164	169
	setup	3 071 s	842 s	432 s
	solve	9 541 s	3 210 s	1 585 s
	total	12 612 s	4 052 s	2 017 s

Albany

https://github.com/SNLComputation/Albany

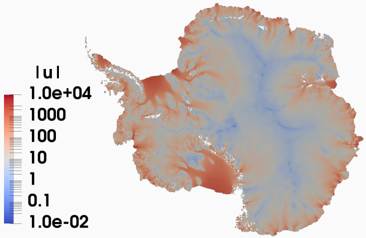

The velocity of the ice sheet in Antarctica and Greenland is modeled by a **first-order-accurate Stokes approximation model**,

$$-\nabla \cdot (2\mu\dot{\epsilon}_1) + \rho g \frac{\partial s}{\partial x} = 0, \quad -\nabla \cdot (2\mu\dot{\epsilon}_2) + \rho g \frac{\partial s}{\partial y} = 0,$$

with a **nonlinear viscosity model** (Glen's law); cf., e.g., **Blatter (1995)** and **Pattyn (2003)**.

	Antarctica (**velocity**) 4 km resolution, 20 layers, 35 m dofs			Greenland (**multiphysics vel. & temperature**) 1-10 km resolution, 20 layers, 69 m dofs		
MPI ranks	avg. its	avg. setup	avg. solve	avg. its	avg. setup	avg. solve
512	**41.9** (11)	25.10 s	12.29 s	**41.3** (36)	18.78 s	4.99 s
1 024	**43.3** (11)	9.18 s	5.85 s	**53.0** (29)	8.68 s	4.22 s
2 048	**41.4** (11)	4.15 s	2.63 s	**62.2** (86)	4.47 s	4.23 s
4 096	**41.2** (11)	1.66 s	1.49 s	**68.9** (40)	2.52 s	2.86 s
8 192	**40.2** (11)	1.26 s	1.06 s	-	-	-

Computations performed on Cori (NERSC).

Heinlein, Perego, Rajamanickam (2022)

Multilevel Domain Decomposition for Neural Networks

Domain Decomposition Methods and Machine Learning – Literature

A **non-exhaustive literature overview**:

- **Machine Learning for adaptive BDDC, FETI–DP, and AGDSW**: Heinlein, Klawonn, Lanser, Weber (2019, 2020, 2021, 2021, 2021, 2022); Klawonn, Lanser, Weber (2024)
- **cPINNs, XPINNs**: Jagtap, Kharazmi, Karniadakis (2020); Jagtap, Karniadakis (2020)
- **Classical Schwarz iteration for PINNs or DeepRitz (D3M, DeepDDM, etc)**: Li, Tang, Wu, and Liao (2019); Li, Xiang, Xu (2020); Mercier, Gratton, Boudier (arXiv 2021); Li, Wang, Cui, Xiang, Xu (2023); Sun, Xu, Yi (arXiv 2022, arXiv 2023); Kim, Yang (2022, arXiv 2023)
- **FBPINNs**: Moseley, Markham, and Nissen-Meyer (2023); Dolean, Heinlein, Mishra, Moseley (2024, acc. 2024 / arXiv:2306.05486); Heinlein, Howard, Beecroft, Stinis (subm. 2024 / arXiv:2401.07888)
- **DDMs for CNNs**: Gu, Zhang, Liu, Cai (2022); Lee, Park, Lee (2022); Klawonn, Lanser, Weber (acc. 2024); Verburg, Heinlein, Cyr (in prep.)

An overview of the state-of-the-art in **early 2021**:

A. Heinlein, A. Klawonn, M. Lanser, J. Weber

Combining machine learning and domain decomposition methods for the solution of partial differential equations — A review

GAMM-Mitteilungen. 2021.

An overview of the state-of-the-art in the **end of 2023**:

A. Klawonn, M. Lanser, J. Weber

Machine learning and domain decomposition methods — A survey

arXiv:2312.14050. 2023

Physics-Informed Neural Networks (PINNs)

In the **physics-informed neural network (PINN)** approach introduced by **Raissi et al. (2019)**, a **neural network** is employed to **discretize a partial differential equation**

$$\mathcal{N}[u] = f, \quad \text{in } \Omega.$$

PINNs use a **hybrid loss function**:

$$\mathcal{L}(\boldsymbol{\theta}) = \omega_{\text{data}} \mathcal{L}_{\text{data}}(\boldsymbol{\theta}) + \omega_{\text{PDE}} \mathcal{L}_{\text{PDE}}(\boldsymbol{\theta}),$$

where ω_{data} and ω_{PDE} are **weights** and

$$\mathcal{L}_{\text{data}}(\boldsymbol{\theta}) = \frac{1}{N_{\text{data}}} \sum_{i=1}^{N_{\text{data}}} \left(u(\hat{\mathbf{x}}_i, \boldsymbol{\theta}) - u_i \right)^2,$$

$$\mathcal{L}_{\text{PDE}}(\boldsymbol{\theta}) = \frac{1}{N_{\text{PDE}}} \sum_{i=1}^{N_{\text{PDE}}} \left(\mathcal{N}[u](\mathbf{x}_i, \boldsymbol{\theta}) - f(\mathbf{x}_i) \right)^2.$$

See also **Dissanayake and Phan-Thien (1994); Lagaris et al. (1998)**.

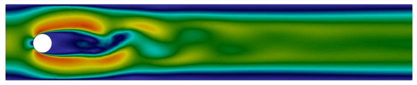

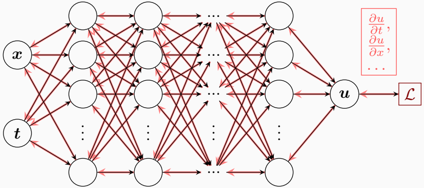

Advantages

- **"Meshfree"**
- **Small data**
- **Generalization properties**
- **High-dimensional problems**
- **Inverse** and **parameterized problems**

Drawbacks

- **Training cost** and **robustness**
- **Convergence not well-understood**
- **Difficulties with scalability** and **multi-scale problems**

Hybrid loss

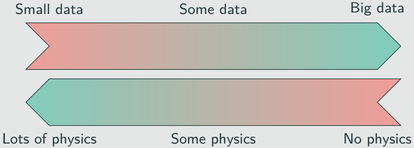

- **Known solution values** can be included in $\mathcal{L}_{\text{data}}$
- **Initial and boundary conditions** are also included in $\mathcal{L}_{\text{data}}$

Solve

$$u' = \cos(\omega \boldsymbol{x}),$$
$$u(0) = 0,$$

for different values of ω using **PINNs with varying network capacities**.

Scaling issues

- Large computational domains
- Small frequencies

Cf. **Moseley, Markham, and Nissen-Meyer (2023)**

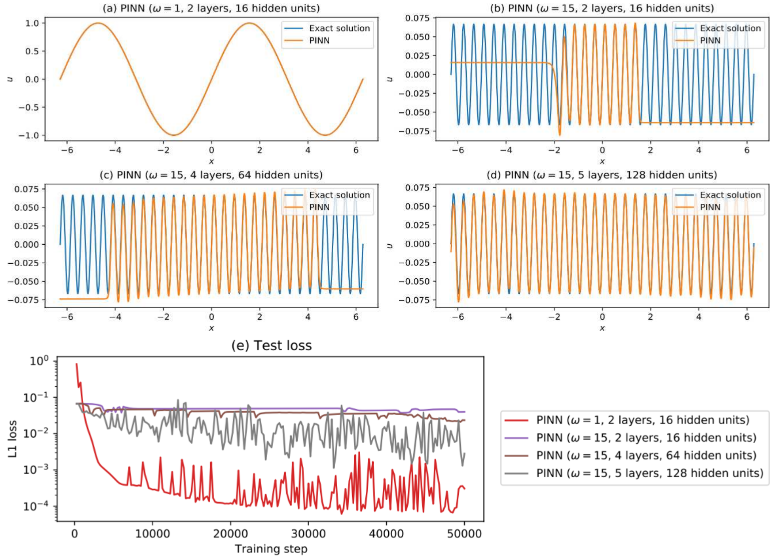

(a) 321 free parameters (d) 66 433 free parameters

Solve

$$\begin{aligned} u' &= \cos(\omega \boldsymbol{x}), \\ u(0) &= 0, \end{aligned}$$

for different values of ω using **PINNs with varying network capacities**.

Scaling issues

- Large computational domains
- Small frequencies

Cf. Moseley, Markham, and Nissen-Meyer (2023)

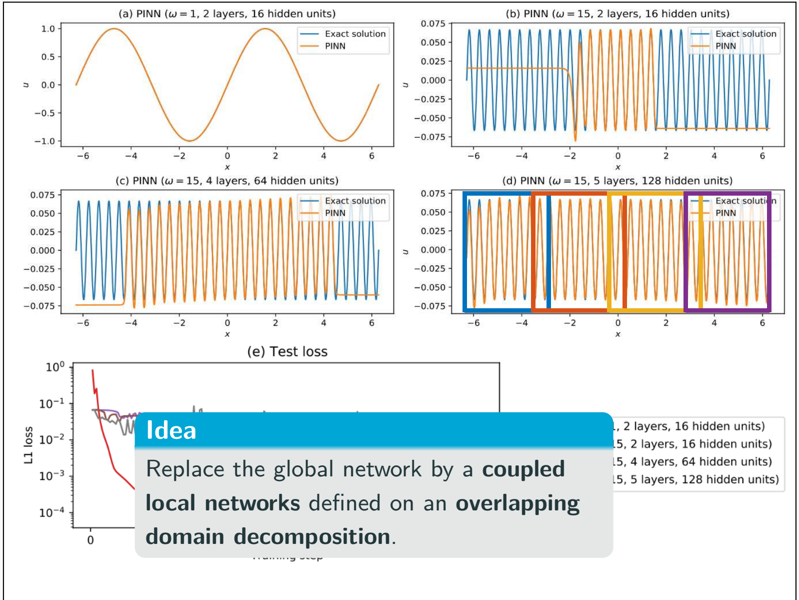

Idea

Replace the global network by a **coupled local networks** defined on an **overlapping domain decomposition**.

(a) 321 free parameters (d) 66 433 free parameters

Finite Basis Physics-Informed Neural Networks (FBPINNs)

In the **finite basis physics informed neural network (FBPINNs) method** introduced in **Moseley, Markham, and Nissen-Meyer (2023)**, we employ the **PINN** approach and **hard enforcement of the boundary conditions**; cf. **Lagaris et al. (1998)**.

FBPINNs use the **network architecture**

$$u(\boldsymbol{\theta}_1, \ldots, \boldsymbol{\theta}_J) = \mathcal{C} \sum\nolimits_{j=1}^{J} \omega_j u_j (\boldsymbol{\theta}_j)$$

and the **loss function**

$$\mathcal{L}(\boldsymbol{\theta}_1, \ldots, \boldsymbol{\theta}_J) = \frac{1}{N} \sum_{i=1}^{N} \Big(\mathcal{N}[\mathcal{C} \sum_{\boldsymbol{x}_i \in \Omega_j} \omega_j u_j](\boldsymbol{x}_i, \boldsymbol{\theta}_j) - f(\boldsymbol{x}_i) \Big)^2.$$

Here:

- **Overlapping DD**: $\Omega = \bigcup_{l=1}^{J} \Omega_j$
- **Partition of unity** ω_j with $\mathrm{supp}(\omega_j) \subset \Omega_j$ and $\sum_{j=1}^{J} \omega_j \equiv 1$ on Ω

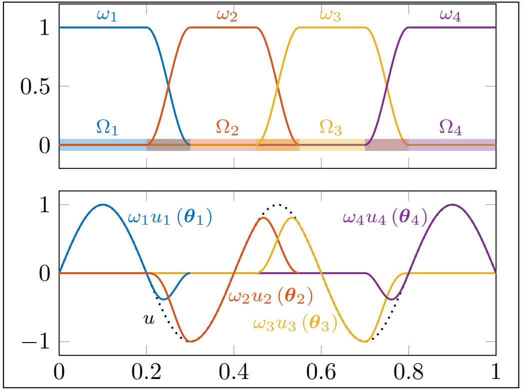

Hard enf. of boundary conditions

Loss function

$$\mathcal{L}(\boldsymbol{\theta}) = \frac{1}{N} \sum\nolimits_{i=1}^{N} \left(\mathcal{N}[\mathcal{C} u](\boldsymbol{x}_i, \boldsymbol{\theta}) - f(\boldsymbol{x}_i) \right)^2,$$

with constraining operator $\mathcal{C}$, which **explicitly enforces the boundary conditions**.

PINN vs FBPINN (Moseley et al. (2023))

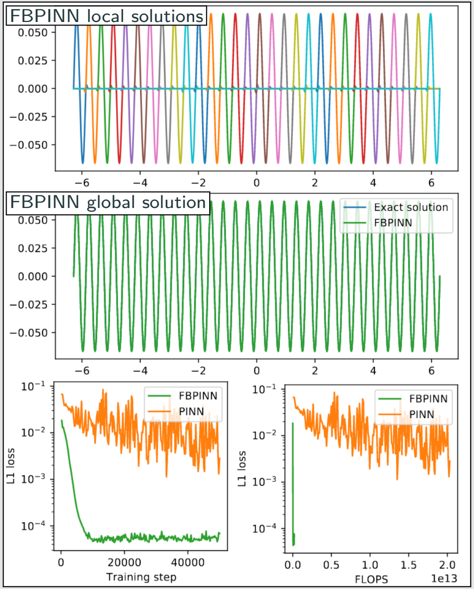

Scalability of FBPINNs

Consider the **simple boundary value problem**

$$-u'' = 1 \text{ in } [0,1],$$

$$u(0) = u(1) = 0,$$

which has the **solution**

$$u(x) = 1/2\, x(1-x).$$

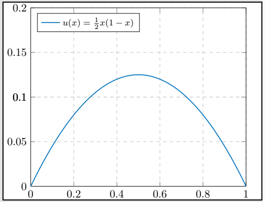

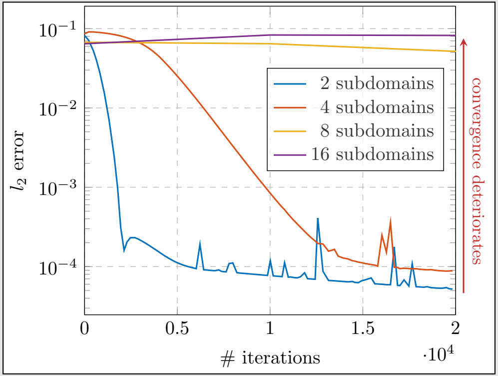

Multi-Level FBPINN Algorithm

Extension of FBPINNs to L levels; Cf. **Dolean, Heinlein, Mishra, Moseley (accepted 2024 / arXiv:2306.05486)**.

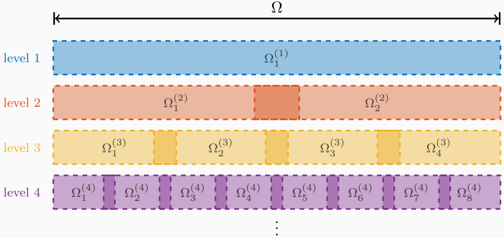

L-level network architecture

$$u\left(\theta_1^{(1)},\ldots,\theta_{J^{(L)}}^{(L)}\right) = \mathcal{C}\left(\sum_{l=1}^{L}\sum_{i=1}^{N^{(l)}}\omega_j^{(l)}u_j^{(l)}\left(\theta_j^{(l)}\right)\right)$$

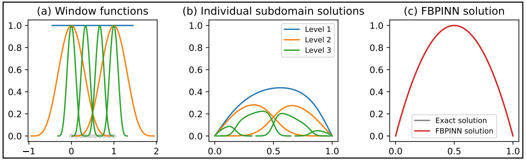

Multi-Frequency Problem

Let us now consider the **two-dimensional multi-frequency Laplace boundary value problem**

$$\begin{aligned} -\Delta u &= 2\sum_{i=1}^{n}(\omega_i\pi)^2\sin(\omega_i\pi x)\sin(\omega_i\pi y) && \text{in } \Omega,\\ u &= 0 && \text{on } \partial\Omega, \end{aligned}$$

with $\omega_i = 2^i$.

For increasing values of n, we obtain the **analytical solutions**:

Multi-Level FBPINN Algorithm

Extension of FBPINNs to L levels; Cf. **Dolean, Heinlein, Mishra, Moseley (accepted 2024 / arXiv:2306.05486)**.

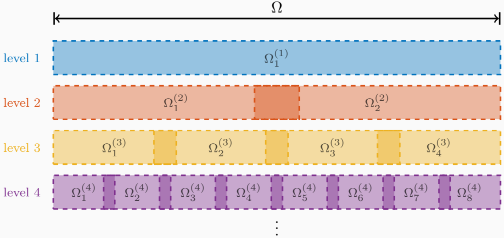

L-level network architecture

$$
u\left(\theta_1^{(1)}, \ldots, \theta_{J^{(L)}}^{(L)}\right) = \mathcal{C}\left(\sum_{l=1}^{L} \sum_{i=1}^{N^{(l)}} \omega_j^{(l)} u_j^{(l)}\left(\theta_j^{(l)}\right)\right)
$$

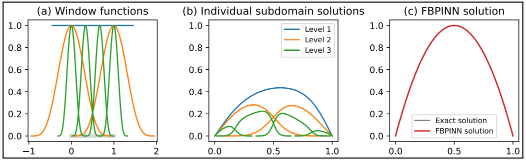

Multi-Frequency Problem

Let us now consider the **two-dimensional multi-frequency Laplace boundary value problem**

$$
\begin{aligned}
-\Delta u &= 2 \sum_{i=1}^{n} (\omega_i \pi)^2 \sin(\omega_i \pi x) \sin(\omega_i \pi y) && \text{in } \Omega, \\
u &= 0 && \text{on } \partial\Omega,
\end{aligned}
$$

with $\omega_i = 2^i$.

For increasing values of n, we obtain the **analytical solutions**:

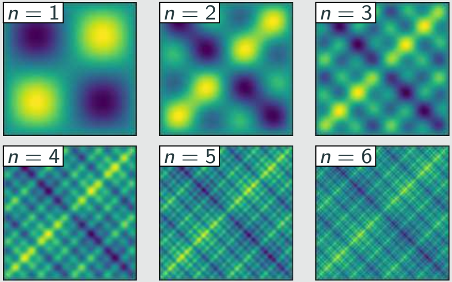

Multi-Level FBPINNs for a Multi-Frequency Problem – Strong Scaling

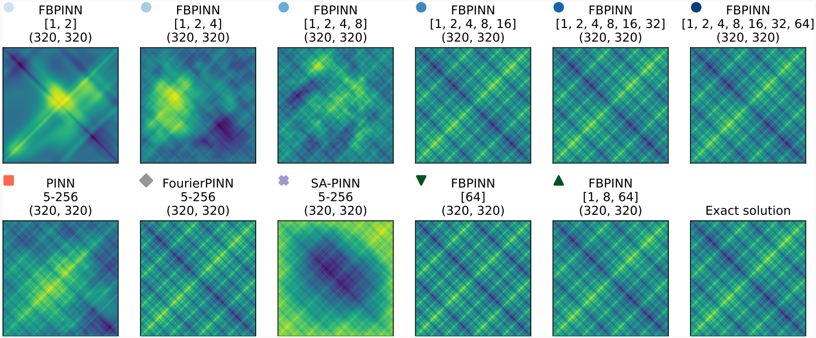

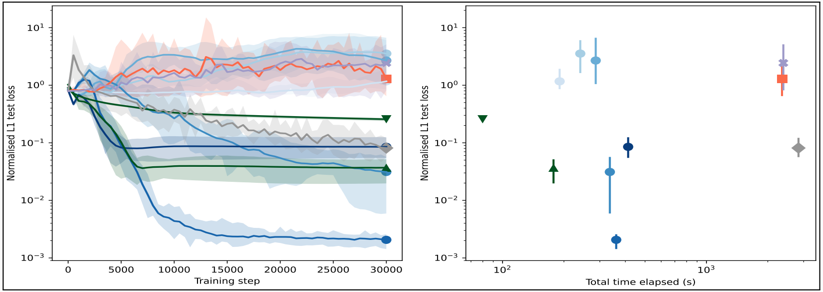

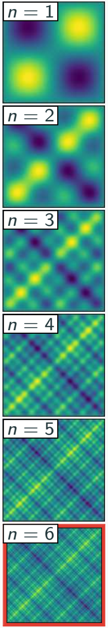

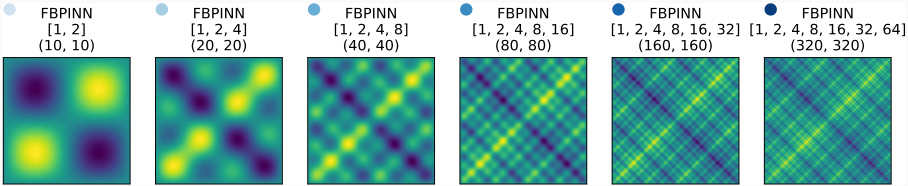

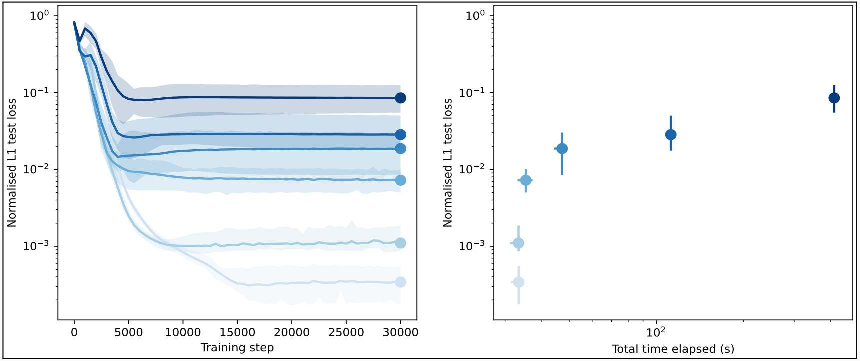

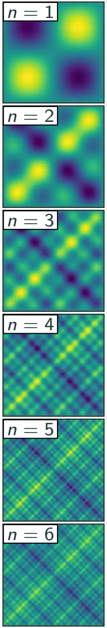

- Ongoing: **analysis and improvement of the convergence**

Cf. **Dolean, Heinlein, Mishra, Moseley (accepted 2024 / arXiv:2306.05486)**. Implementation using JAX

Memory Requirements for CNN Training

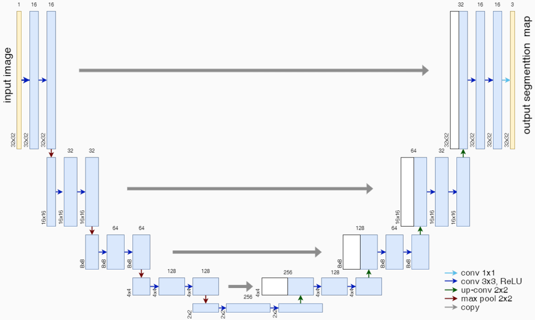

- As an example for a **convolutional neural network (CNN)**, we employ the **U-Net architecture** introduced in **Ronneberger, Fischer, and Brox (2015)**.
- The U-Net yields **state-of-the-art accuracy in semantic image segmentation** and other **image-to-image tasks**.

Below: *memory consumption for training on a single* 1024×1024 *image.*

name	**size**	**# channels**		**mem. feature maps**		**mem. weights**	
		input	**output**	**# of values**	**MB**	**# of values**	**MB**
input block	1 024	3	64	268 M	**1 024.0**	38 848	**0.148**
encoder block 1	512	64	128	167 M	**704.0**	221 696	**0.846**
encoder block 2	256	128	256	84 M	**352.0**	885 760	**3.379**
encoder block 3	128	256	512	42 M	**176.0**	3 540 992	**13.508**
encoder block 4	64	512	1 024	21 M	**88.0**	14 159 872	**54.016**
decoder block 1	64	1,024	512	50 M	**192.0**	9 177 088	**35.008**
decoder block 2	128	512	256	101 M	**384.0**	2 294 784	**8.754**
decoder block 3	256	256	128	201 M	**768.0**	573 952	**2.189**
decoder block 4	512	128	64	402 M	**1 536.0**	143 616	**0.548**
output block	1 024	64	3	3.1 M	**12.0**	195	**0.001**

Decomposing the U-Net

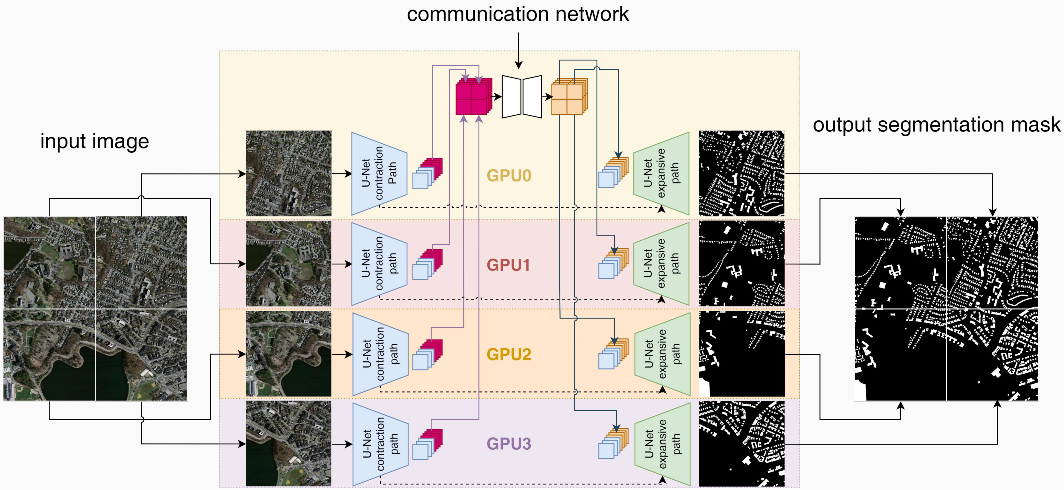

Cf. **Verburg, Heinlein, Cyr (in preparation).**

Decomposing the U-Net

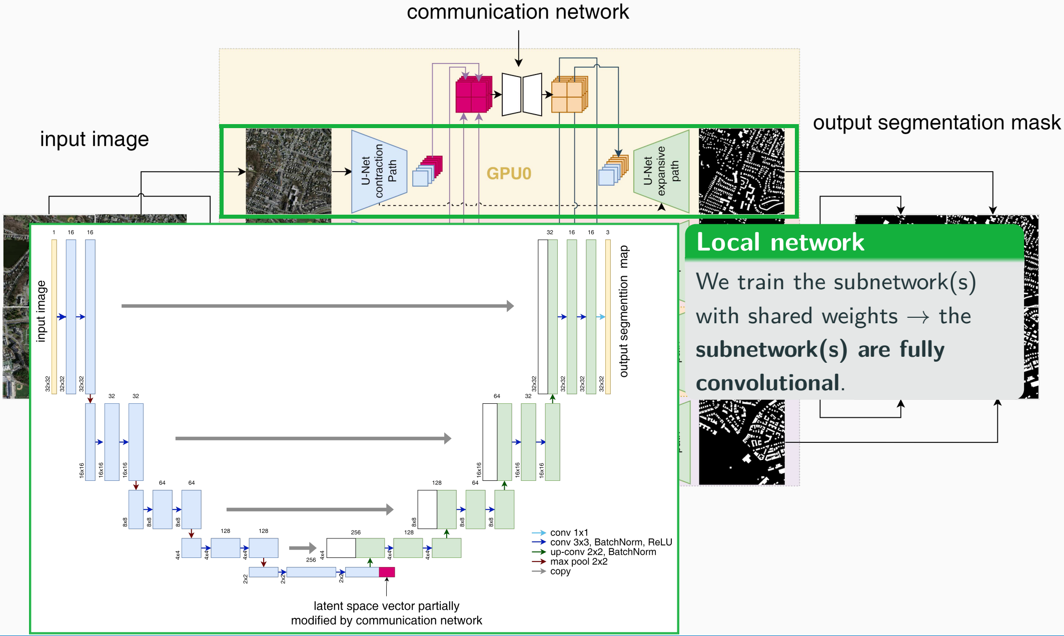

Local network

We train the subnetwork(s) with shared weights → the **subnetwork(s) are fully convolutional**.

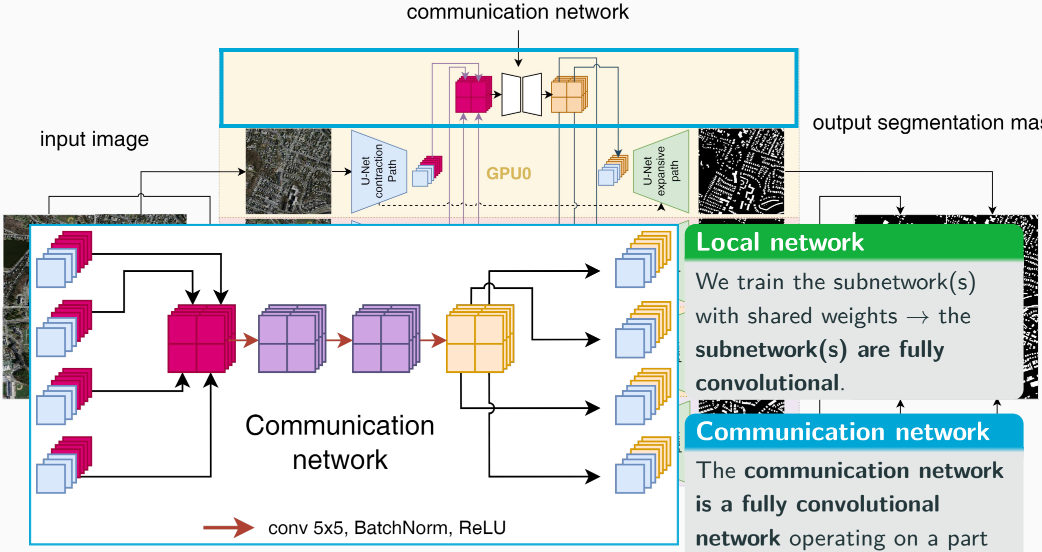

Local network

We train the subnetwork(s) with shared weights → the **subnetwork(s) are fully convolutional**.

Communication network

The **communication network is a fully convolutional network** operating on a part of the coarse feature maps.

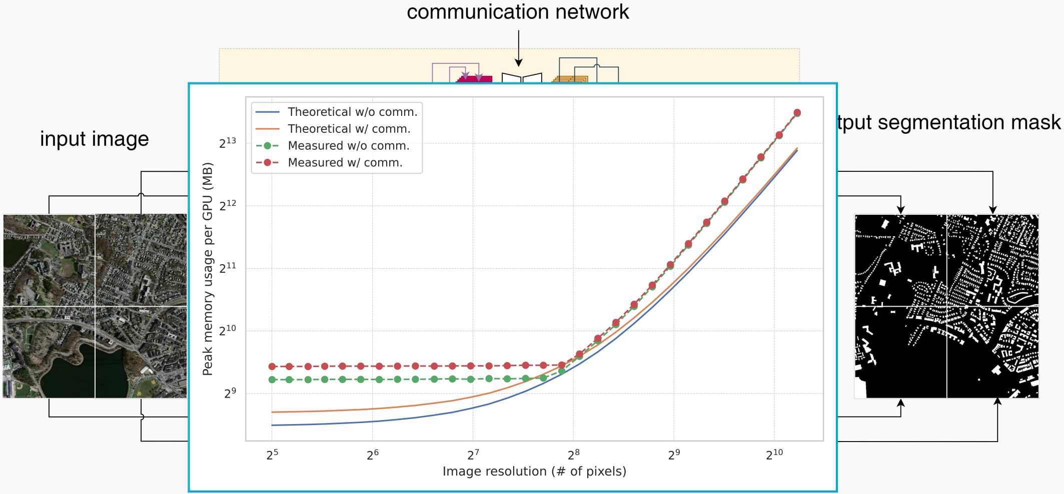

- Distribution of feature maps results in **significant reduction of memory usage on a single GPU**
- **Moderate additional memory usage** due to the **communication network**

Task: Connect two dots via a line segment

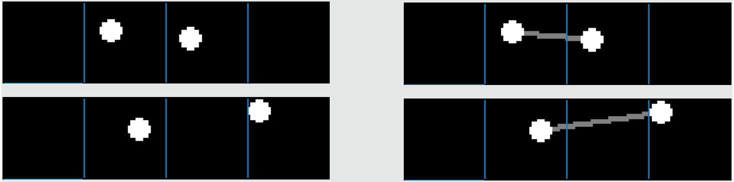

Result: Communication

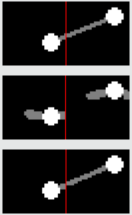

Training & testing on # of subimages (32 × 32 pixels) vs. # feature maps communicated

# subimages	0	1	2	4	8	16	32	Baseline
2	0.14	0.55	0.57	0.87	0.91	0.92	0.93	0.95
3	0.14	0.44	0.66	0.77	0.84	0.90	0.92	0.81
4	0.14	0.58	0.61	0.77	0.84	0.88	0.90	0.74
6	0.14	0.23	0.54	0.67	0.72	0.82	0.87	0.68
8	0.14	0.18	0.40	0.50	0.63	0.70	0.69	0.39
16	0.08	0.18	0.18	0.18	0.18	0.18	0.20	0.19

Testing on 6 subimages

Training on # subimages (32 × 32 pixels) vs. # feature maps communicated

# subimages	0	1	2	4	8	16	32	Baseline
2	0.13	0.20	0.20	0.29	0.28	0.30	0.40	0.53
3	0.14	0.39	0.65	0.75	0.79	0.88	0.92	0.76
4	0.14	0.59	0.55	0.77	0.78	0.83	0.73	0.75
6	0.14	0.23	0.54	0.67	0.72	0.82	0.87	0.68
8	0.13	0.18	0.39	0.49	0.64	0.71	0.70	0.42
16	0.13	0.14	0.14	0.16	0.18	0.16	0.26	0.26

DeepGlobe 2018 Satellite Image Data Set (Demir et al. (2018))

class	pixel count	proportion
urban	642.4M	9.35 %
agriculture	3898.0M	56.76 %
rangeland	701.1M	10.21 %
forest	944.4M	13.75 %
water	256.9M	3.74 %
barren	421.8M	6.14 %
unknown	3.0M	0.04 %

Input **Target**

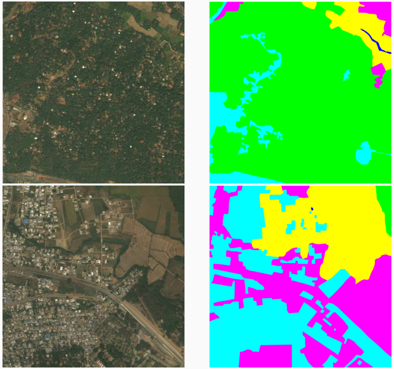

Avoiding overfitting

The data set includes **only** 803 **images**. To **avoid overfitting**, we

- apply **batch normalization** and use **random dropout** layers and **data augmentation**
- **initialize the encoder** using the **ResNet-18** (**He, Zhang, Ren, and Sun(2016)**)

image **true mask** **without comm.** **with comm.**

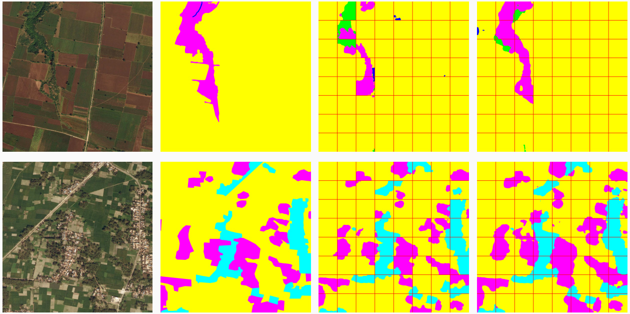

DeepGlobe 2018 Satellite Image Data Set (Demir et al. (2018))

class	pixel count	proportion
urban	642.4M	9.35 %
agriculture	3898.0M	56.76 %
rangeland	701.1M	10.21 %
forest	944.4M	13.75 %
water	256.9M	3.74 %
barren	421.8M	6.14 %
unknown	3.0M	0.04 %

Input **Target**

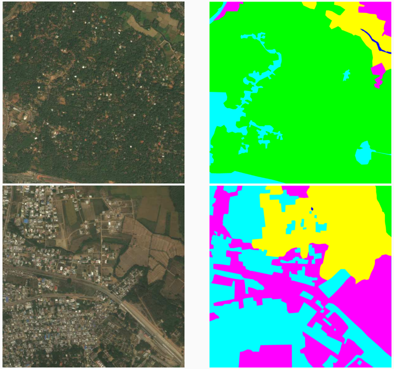

Avoiding overfitting

The data set includes **only 803 images**. To **avoid overfitting**, we

- apply **batch normalization** and use **random dropout** layers and **data augmentation**
- **initialize the encoder** using the **ResNet-18** (**He, Zhang, Ren, and Sun(2016)**)

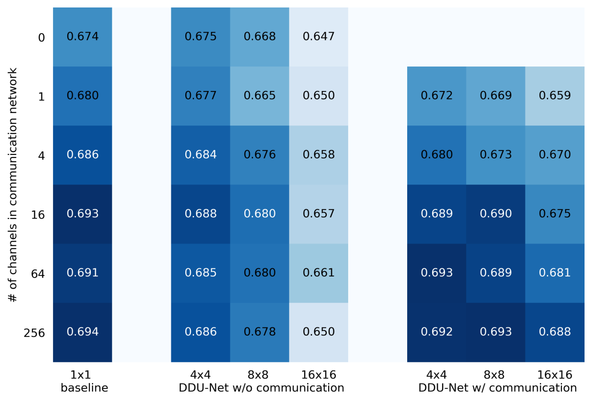

Coarse levels for domain decomposition methods

- **Numerical scalability** and **robust convergence** for
  - **heterogeneous** problems
  - **multiphysics** problems
  - **highly nonlinear** problems
- **Representation** of **coarse scale features**
- **Fast transport** of **global information**
- **Challenges**:
  - Implementation is often **intrusive**
  - **Bottleneck** for **parallel scalability**

→ **Algebraic** and **parallel** implementation in FROSch

Acknowledgements

- **Financial support:** DFG (KL2094/3-1, RH122/4-1), DFG SPP 2311 project number 465228106, DOE SciDAC-5 FASTMath Institute (Contract no. DE-AC02-05CH11231)
- **Computing resources:** Summit (OLCF), Cori (NERSC), magnitUDE (UDE), Piz Daint (CSCS), Fritz (FAU), DelftBlue (TU Delft)

Thank you for your attention!